Supplementary Information

A highly conductive and ultra-stretchable polyaniline/cellulose nanocrystal/polyacrylamide hydrogel with hydrophobic associations for wearable strain sensors

Pooria Rahmani[a,b], Akbar Shojaei[a*], Michael D. Dickey[b*]

[a] Department of Chemical and Petroleum Engineering, Sharif University of Technology,

PO Box 11155-9465, Tehran, Iran

[b] Department of Chemical and Biomolecular Engineering, North Carolina State University, Raleigh, North Carolina 27695-7905, United States

* Corresponding authors

Email addresses: akbar.shojaei@sharif.edu (A. Shojaei); mddickey@ncsu.edu (M. D. Dickey)

Characterization of the CNC synthesized in this work

Field emission scanning electron microscopy (FE-SEM) and noncontact atomic force microscopy (AFM) images of CNCs (**Figs. S1, 2)**, reveal that they have rod-like shape with relatively high aspect ratio, whose length (~200 nm) is several times larger than their diameter (~20 nm) [1]. According to thermogravimetric analysis (TGA) and derivative thermogravimetry (DTG) (**Fig. S3**), CNC undergoes thermal decomposition via two pyrolysis processes, which are within the range of ≈ 200-300 °C (dominant) and ≈ 300-550 °C, consistent with literature [2, 3]. As expected, the Fourier transform infrared (FTIR) spectra of CNC has peaks at wavelengths of 2904 and 1061 cm^{-1}, attributed to vibrations of C-H and C-O stretching, respectively. Meanwhile, the sharp peak at 3350 cm^{-1} is assigned to O-H stretching vibration (**Fig. S4**) [2]. According to XRD spectra of

CNC (**Fig. S5**), the peaks at around degrees of 14.7°, 22.5°, and 34.4° are corresponded to crystal planes of 110, 200, and 004, respectively, in accordance to the literature [4].

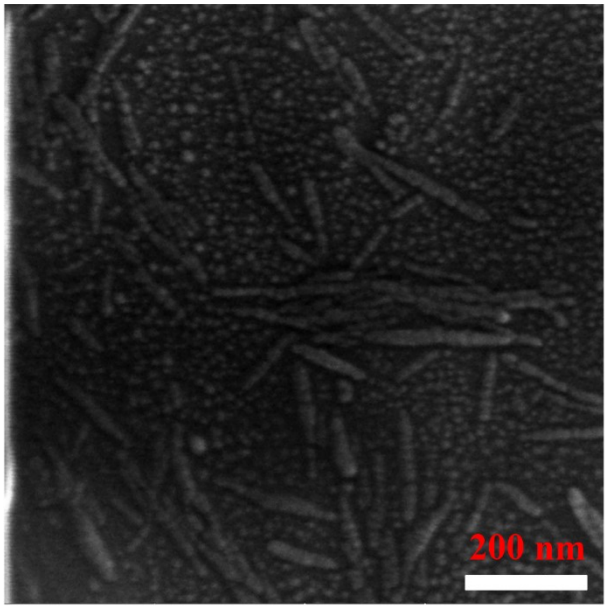

Fig. S1. FE-SEM image of CNCs.

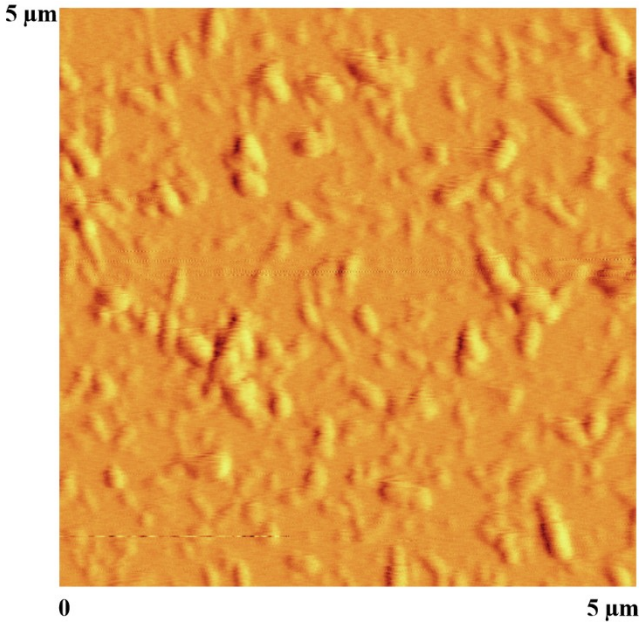

Fig. S2. Topographic image of CNC provided by AFM.

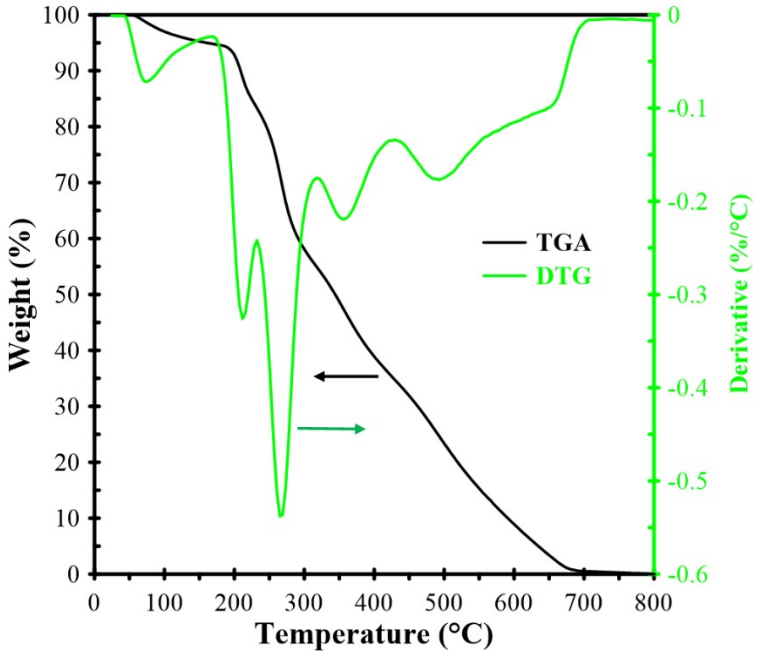

Fig. S3. TGA (right axis) and DTG (left axis, colored by green) plots of CNC.

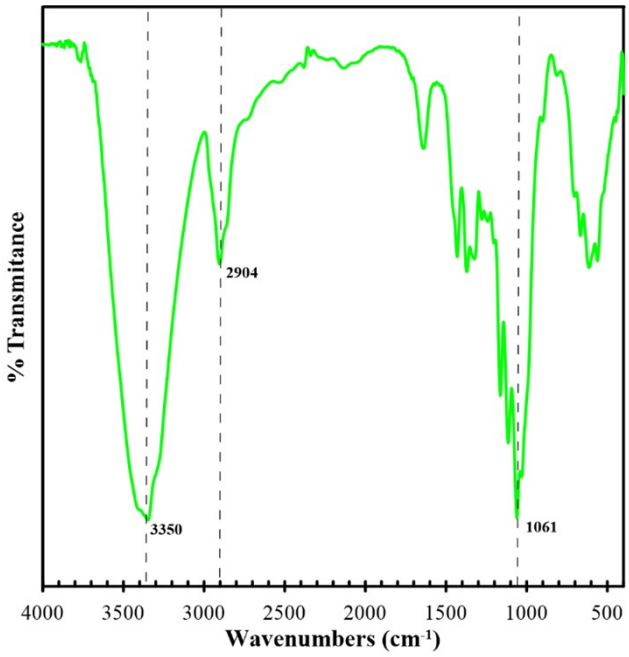

Fig. S4. FTIR spectrum of CNC.

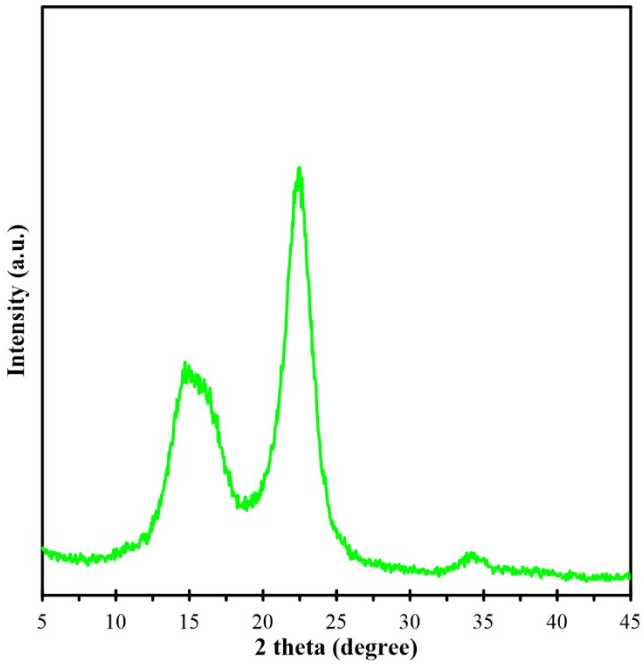

Fig. S5. XRD spectrum of CNC.

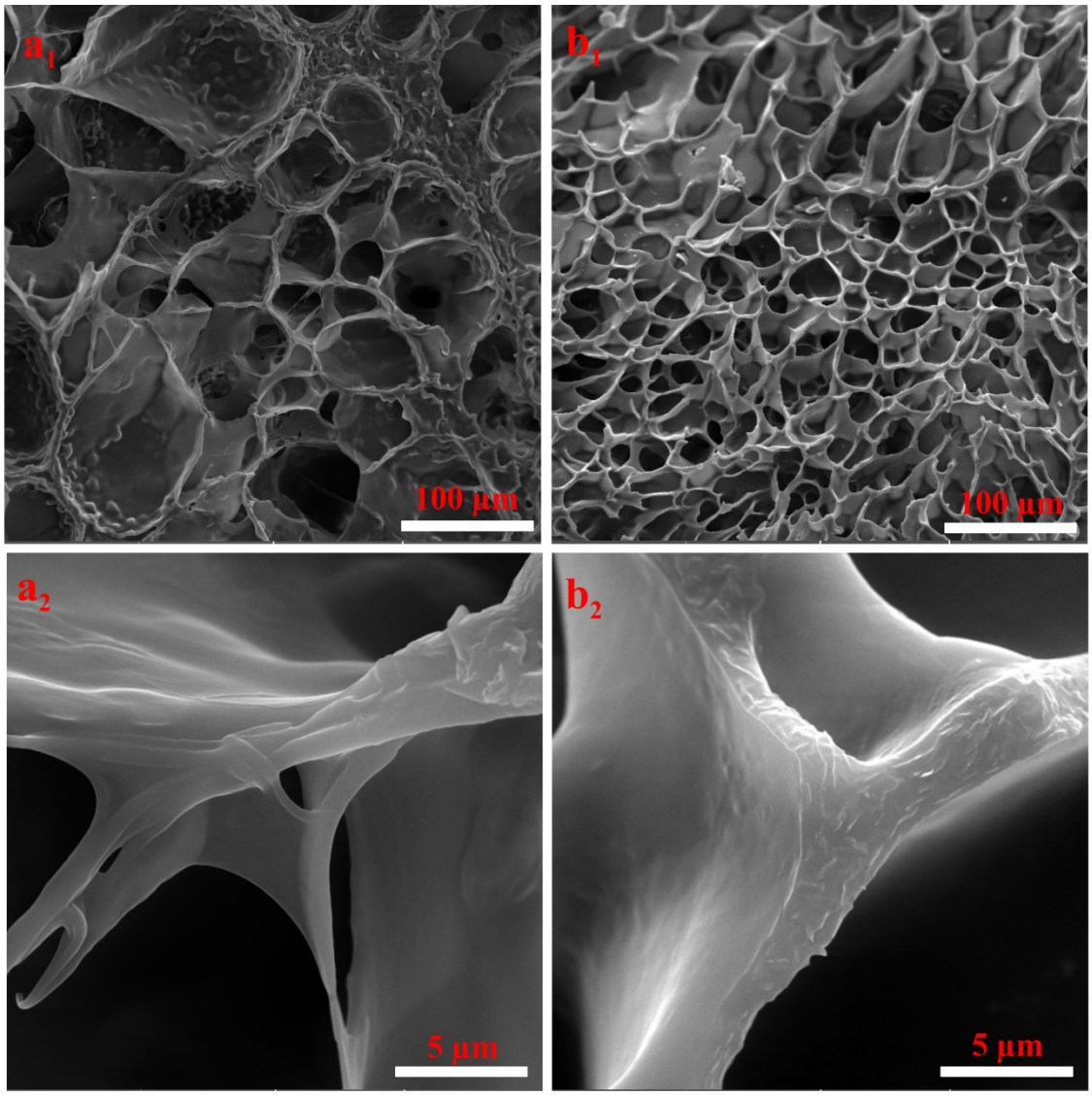

Fig. S6. FE-SEM images of pure HAPAAm at the scales of a_1) 100 µm and a_2) 5 µm and HAPAAm/CNC at same scales of b_1) 100 µm and b_2) 5 µm. Pore walls of HAPAAm/CNCs (image b_2) have more roughness than that of HAPAAm (image a_2).

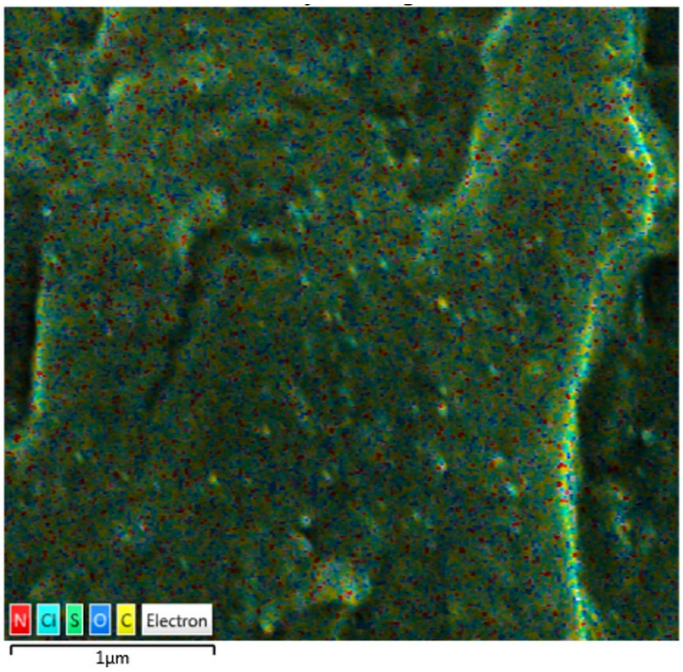

Fig. S7. EDS-SEM of HAPAAm/CNC/PAni0.5. Tracking the location and percentage of Cl elements gives helpful data regarding the presence of PAni; since protonated aniline is doped with Cl (from HCl) during aniline in-situ polymerization. Cl elements, colored in light blue, has been disturbed well within the gel with the mass percentage of 4.78%. We rule out the presence of mobile (undoped) Cl ions within the gel; since the HAPAAm/CNC/PAni0.5 M gel was immersed into the water, followed by into the H_3PO_4 (1M) after soaking process for removing impurities (ions, unreacted monomers).

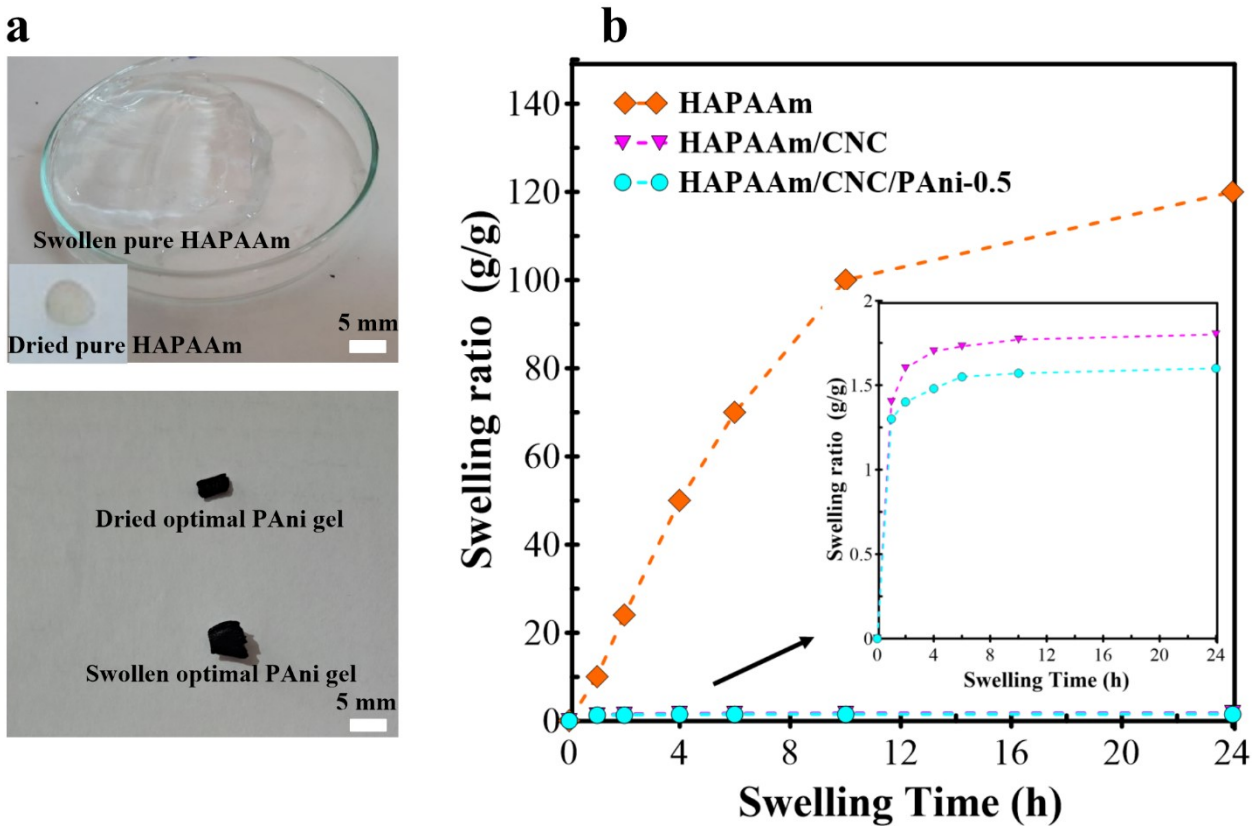

Fig. S8. a) Photographs showing the swelling of HAPAAm and HAPAAm/CNC/PAni-0.5 after one day immersion in DI water. b) Comparison the swelling ratio of HAPAAm, HAPAAm/CNC, and HAPAAm/CNC/PAni-0.5 after one day immersion in DI water

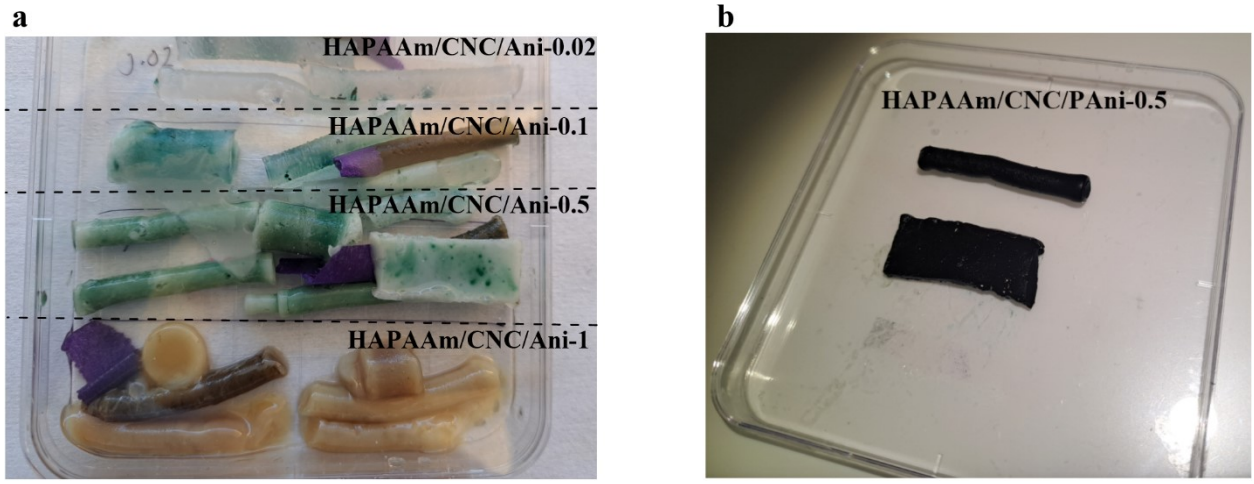

Fig. S9. a) Photographs showing the hydrogels after immersion into acidic aniline solutions with different concentrations. b) Photograph of optimal hydrogel (HAPAAm/CNC/PAni-0.5), obtained after immersion of HAPAAm/CNC/Aniline (Ani)-0.5 in 0.5 M acidic APS solution.

Table S1. The second column presents swelling degree of HAPAAm/CNC hydrogels after immersion in acidic solution containing aniline and APS with different concentrations. The rise in aniline content up to 0.5 M decreases the immersion-induced swelling. The third column shows the equilibrium water content of HAPAAm/CNC/PAni hydrogels. The fourth column shows the tuned water content of HAPAAm/CNC/PAni hydrogels (after their excess water is removed by heating). The rise in aniline content up to 0.5 M decreases the final water content. Note that the mass percentage of water in precursor solution of HAPAAm/CNC was around 72.

Sample	Swelling degree (g/g)	$(\text{Water content})_{\text{equilibrium}}$ (%)	$(\text{Water content})_{\text{tuned}}$ (%)
HAPAAm/CNC	-	-	72
HAPAAm/CNC/PAni-0.02	1.50	88	85
HAPAAm/CNC/PAni-0.1	1.05	86	81
HAPAAm/CNC/PAni-0.5	0.99	85	76
HAPAAm/CNC/PAni-1	0.70	83	75

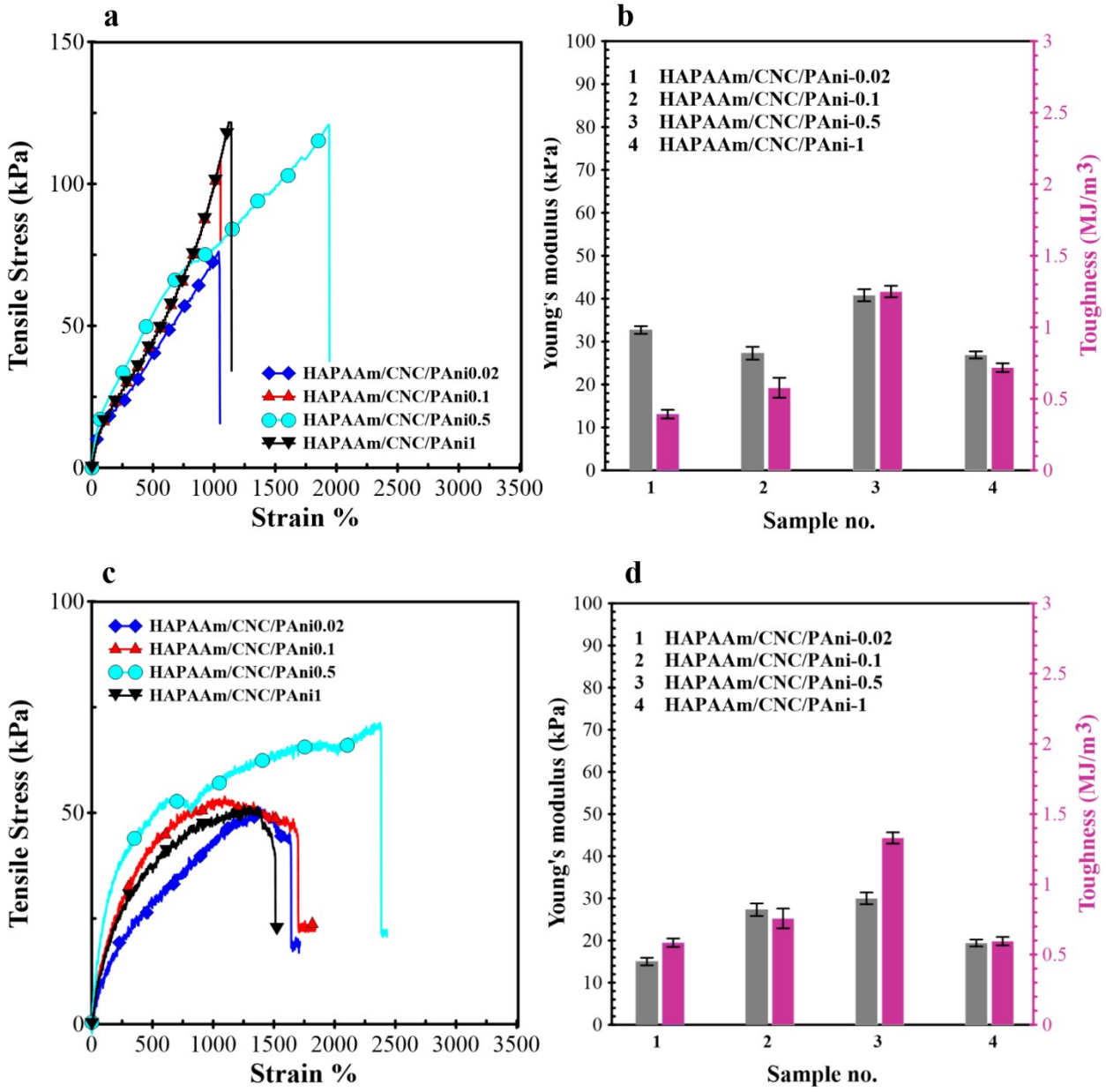

Fig. S10. Tensile stress-strain plot and Young's modulus and toughness of HAPAAm/CNC/PAni hydrogels with equilibrium water content (a and b, respectively) and with tuned water content through heating the gels at 90 °C for 1h (c and d, respectively).

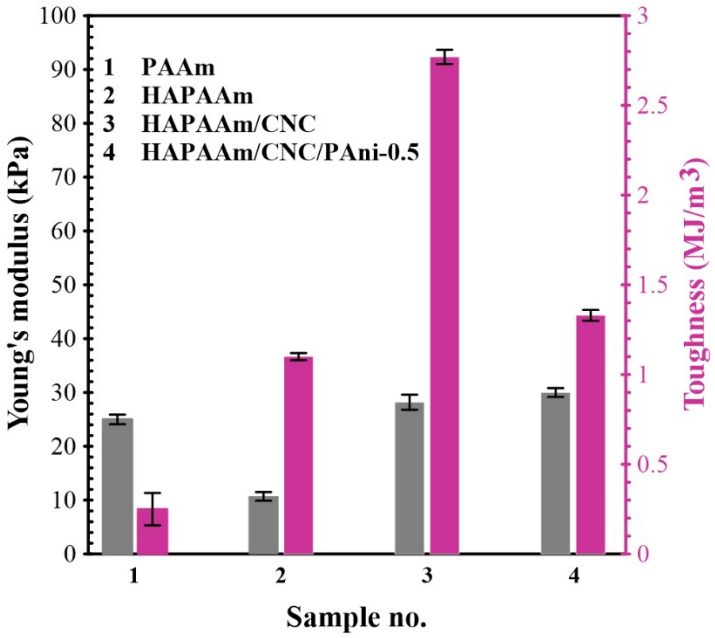

Fig. S11. Young's modulus and toughness of PAAm, HAPAAm, HAPAAm/CNC and HAPAAm/CNC/PAni-0.5.

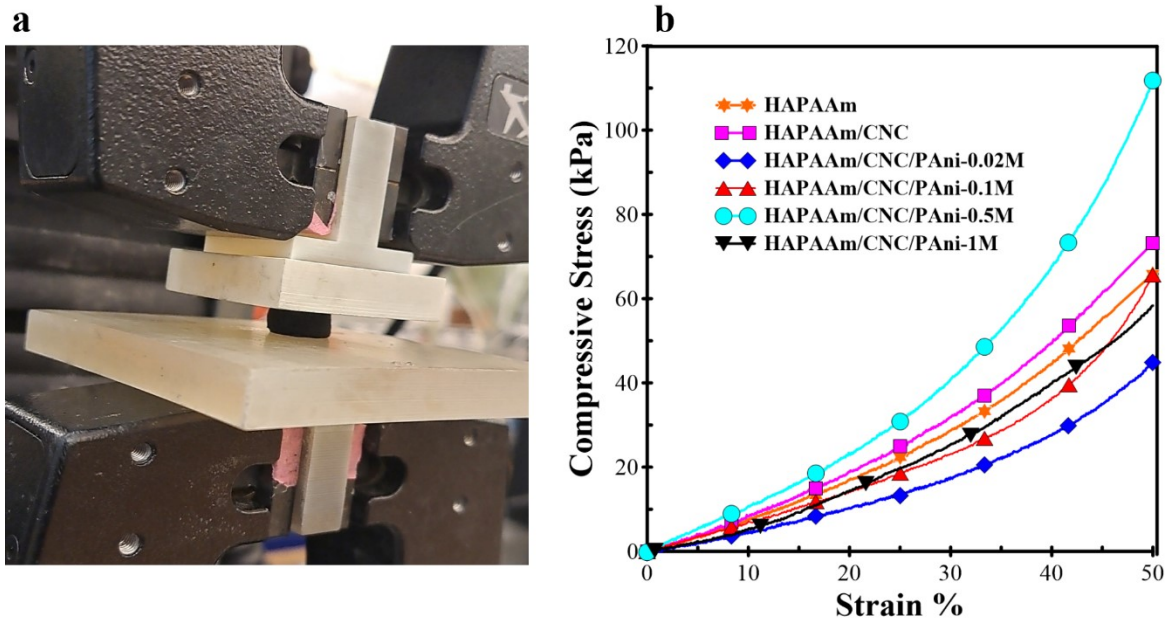

Fig. S12. a) Photograph showing the compression test on the HAPAAm/CNC/PAni-0.5. b) Compressive stress-strain curve of HAPAAm/CNC and HAPAAm/CNC/PAni hydrogels.

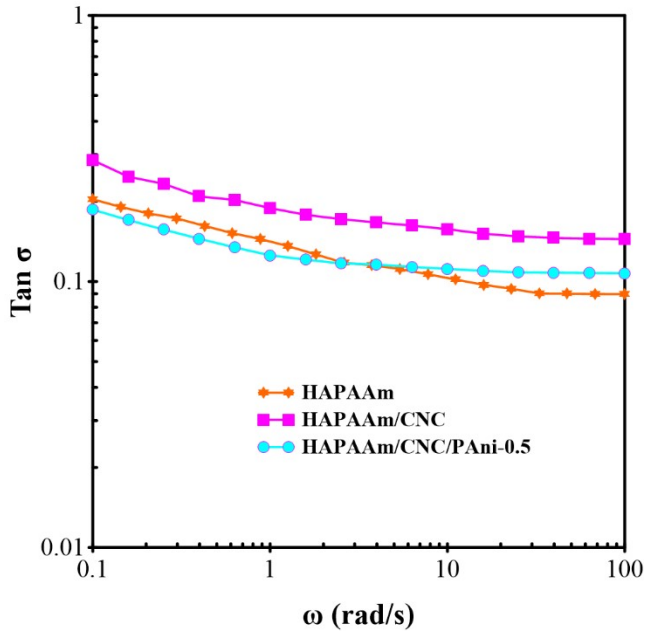

Fig. S13. Tan σ plots of HAPAAm, HAPAAm/CNC, and HAPAAm/CNC/Pani-0.5 as a function of frequency obtained from rheological tests.

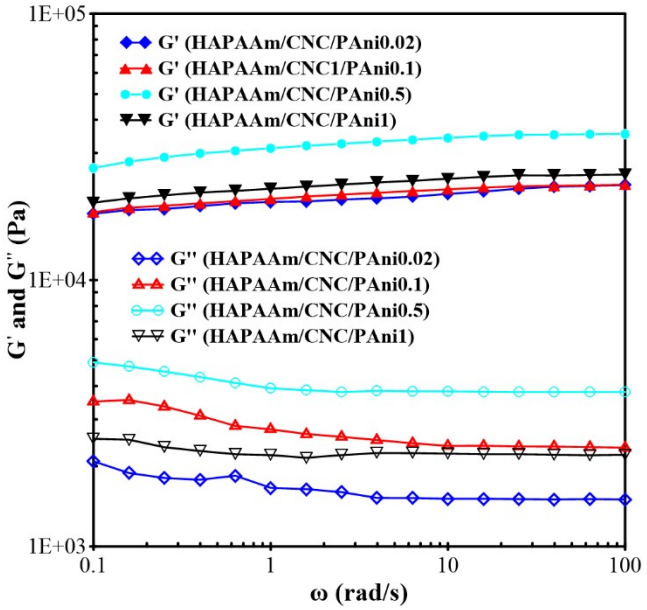

Fig. S14. Frequency sweep of HAPAAm/CNC/PAni hydrogels.

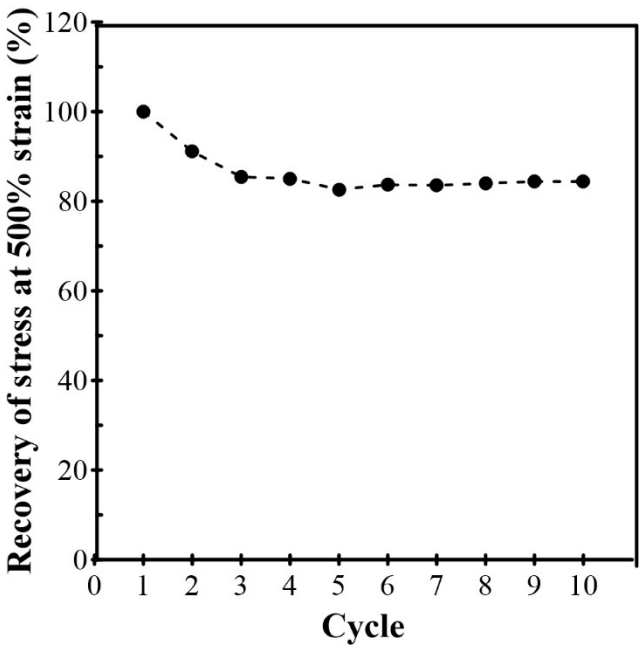

Fig. S15. g) The recovery of stress at 500% strain (defined as the tensile stress at 500% strain for each cycle relative to that of first cycle) of HAPAAm/CNC/PAni-0.5 under 10 successive cyclic stretching at 500%.

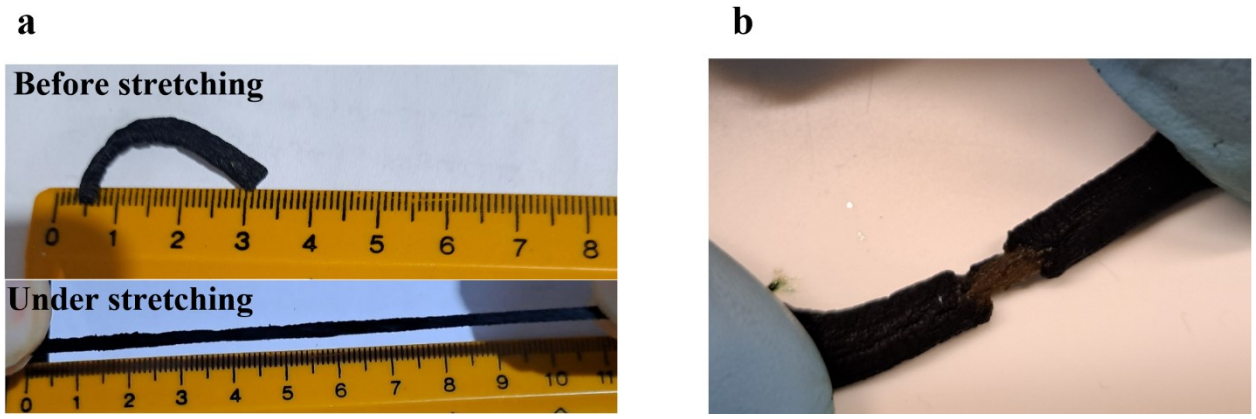

Fig. S16. a) Considerable stretchability of HAPAAm/CNC/PAni-0.5after one day being placed on the hotplate at 90 ˚C. b) Photograph showing that the PAni-rich outer layer covers the hydrogel inner part.

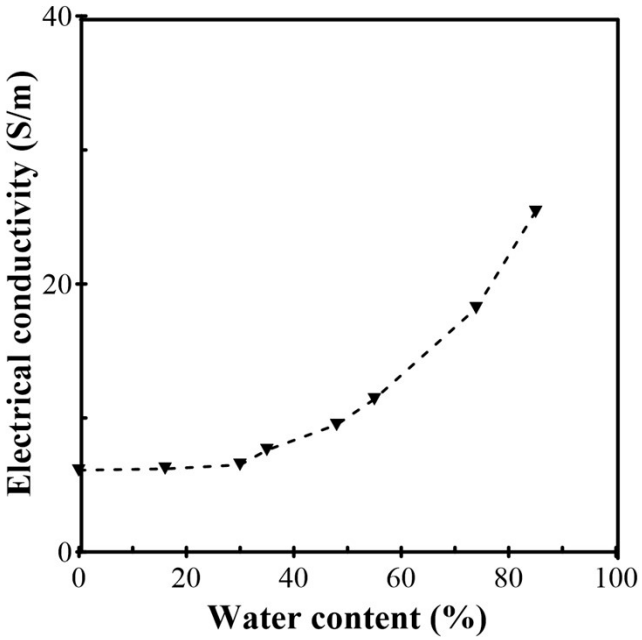

Fig. **S17.** Effect of water content on electrical conductivity of HAPAAm/CNC/PAni0.5. The gel was freeze dried until it totally lost its water. The decrease in water content significantly drops the electrical conductivity of the gel. But, it plateaus at almost constant value (≈ 6.5 S/m) at low water content. We reason that both PAni electronic conductors and mobile ions contribute to the excellent electrical conductivity of HAPAAm/CNC/PAni0.5 at water contents beyond 40%. In comparison, the gel loses its ionic conductivity at low water content (blow 40%) and only PAni nanofibers are responsible for suitable electrical conductivity of the gel in such a condition.

Table S2. Comparison in strain sensing data at low strains (below than 200%) between this work and recent PAni-based hydrogel strain sensors reported in literature.

Materials	**Strain range (%)**	**GF**	**Ref**
HAPAAm/SiO_2-PAni	0-40 40-200	2.27 (linear) 4.37	[5]
PAAm/cellulose/PAni	0-150	1.64	[6]
PVA/PAni	0-107	1.4	[7]
P(AAm-co-DMC)/PAni	0-100	1.6	[8]
P(EG-co-AA)/PAni NPs	0-50 50-200	1.46 2.43	[9]
PAAm/SA/BC/PAni	0-150	0.85	[10]
PU-DA/PAni-Phytic Acid	0-120	2.89, linear (R^2=0.994)	[11]
PNIPAM/CMCS/MWCNT/PANI	0-100	3.6, linear (R^2=0.995)	[12]
PVA/GA/PAni/PA	0-300	3.4	[13]
HAPAAm/CNC/PAni-0.5	**0-200**	**3.7, linear (R^2=0.986)**	**This work**

References:

[1] P. He, R. Guo, K. Hu, K. Liu, S. Lin, H. Wu, L. Huang, L. Chen, Y. Ni, Chemical Engineering Journal 414 (2021) 128726.
[2] M. Yadav, K. Behera, Y.-H. Chang, F.-C. Chiu, Polymers 12 (2020) 202.
[3] N. Wang, E. Ding, R. Cheng, Polymer 48 (2007) 3486-3493.
[4] M. Thakur, A. Sharma, V. Ahlawat, M. Bhattacharya, S. Goswami, Materials Science for Energy Technologies 3 (2020) 328-334.
[5] Y. Li, C. Liu, X. Lv, S. Sun, Soft Matter 17 (2021) 2142-2150.
[6] Y. Li, Q. Gong, X. Liu, Z. Xia, Y. Yang, C. Chen, C. Qian, Carbohydrate Polymers 267 (2021) 118207.
[7] Y. Zhao, B. Zhang, B. Yao, Y. Qiu, Z. Peng, Y. Zhang, Y. Alsaid, I. Frenkel, K. Youssef, Q. Pei, Matter 3 (2020) 1196-1210.
[8] X. Chen, W. Hao, T. Lu, T. Wang, C. Shi, Y. Zhao, Y. Liu, Macromolecular Chemistry and Physics 222 (2021) 2100165.
[9] X. Yu, H. Zhang, Y. Wang, X. Fan, Z. Li, X. Zhang, T. Liu, Advanced Functional Materials 32 (2022) 2204366.
[10] H. Qin, Y. Chen, J. Huang, Q. Wei, Macromolecular Materials and Engineering 306 (2021) 2100159.
[11] Y. Fang, J. Xu, F. Gao, X. Du, Z. Du, X. Cheng, H. Wang, Composites Part B: Engineering 219 (2021) 108965.
[12] T. Zhan, H. Xie, J. Mao, S. Wang, Y. Hu, Z. Guo, ChemistrySelect 6 (2021) 4229-4237.
[13] H. Wei, D. Kong, T. Li, Q. Xue, S. Wang, D. Cui, Y. Huang, L. Wang, S. Hu, T. Wan, ACS sensors 6 (2021) 2938-2951.